



Transformation of CuS/ZnS nanomaterials to an efficient visible light photocatalyst by ‘photosensitizer’ graphene and the potential antimicrobial activities of the nanocomposites

Piu Das¹ · Kartik Tantubay¹ · Raktim Ghosh² · Somasri Dam² · Moni Baskey (Sen)¹

Received: 20 November 2020 / Accepted: 19 April 2021 / Published online: 1 May 2021

© The Author(s), under exclusive licence to Springer-Verlag GmbH Germany, part of Springer Nature 2021

Abstract

We report the growth of CuS/ZnS (CZS) nanoparticles (NPs) on the graphene sheet by a facile green synthesis process. The CuS/ZnS-graphene (CZSG) nanocomposites exhibit enhanced visible light photocatalytic activity towards organic dye (methylene blue) degradation than that of CZS nanoparticles. To find the reason for the enhanced photo-activity, we propose a new photocatalytic mechanism where graphene in the CZSG nanocomposites acts as a ‘photosensitizer’ for CZS nanoparticles. This distinctive photocatalytic mechanism is noticeably different from all other previous research works on semiconductor-graphene hybrid photocatalysts where graphene behaves as an electron reservoir to capture the electrons from photo-excited semiconductor. This novel idea of the photocatalytic mechanism in semiconductor-graphene photocatalysts could draw a new track in thinking for designing of graphene-based photocatalysts for solving environmental pollution problems and they also show remarkable antimicrobial activities.

Keywords Graphene · Photosensitizer · CuS/ZnS NPs · Photocatalyst · Visible light · Antimicrobial activity

Introduction

Graphene-based semiconductor nanocomposites have been considered as one of the ultimate solutions for energy and environmental issues after the discovery of photocatalytic hydrogen production by Fujishima and Honda in 1972 (Fujishima and Honda 1972). Among different environmental issues, water pollution is one of the major problems throughout the whole world (Yek et al. 2020; Nasrollahzadeh et al. 2020). During several years, significant progresses have been built to solve the water pollution problems and numerous nanomaterials have been constructed to be effective for wastewater management by photocatalytic dye degradation (Akbari

et al. 2020; Das et al. 2018; Liang et al. 2017). In contrast, explorations on using graphene-based ternary semiconductor nanocomposites for the photocatalytic reaction are very few. Recently, our group has reported (Tantubay et al. 2020) reduced graphene oxide-CuO/ZnO nanocomposite as an efficient catalyst highlighting an intimate contact that is necessary for the reduction of 4-nitroaniline to p-phenylenediamine.

Notably, several literature surveys show the tremendous photocatalytic applications in the case of ternary nanocomposites or graphene-based hybrid (e.g., CuO/ZnO, CuS/ZnS, CdS/ZnO, CdS/ZnS, ZnO/ZnS) (Prabhu et al. 2019; Feng et al. 2016; Ma et al. 2017; Tang et al. 2015; Lonkar et al. 2018) nanostructures. But there seems to be concurrence that enhancement of photocatalytic activity has been increased after combining the semiconductors with graphene which acts as an electron reservoir to accept the photo-generated electrons from the semiconductor resulting prolonged separation and lifetime between electron-hole pairs and this phenomenon is responsible for photo-activity enhancement. From the past decades, several metal sulfide semiconductor photocatalysts have been proven for wastewater treatment in the presence of different organic dyes or reagents (Wang et al. 2020; Mosleh et al. 2019) due to their visible light response. Among those

Responsible Editor: Sami Rtimi

✉ Moni Baskey (Sen)
moni.baskey@gmail.com

¹ Materials Research Laboratory, Department of Chemistry, The University of Burdwan, Golapbag, Burdwan, West Bengal 713104, India

² Department of Microbiology, The University of Burdwan, Burdwan, West Bengal 713104, India

photocatalysts, ZnS is a typical IIB–VIA group (Feng et al. 2016) semiconductor photocatalyst which exhibits a 90% quantum yield at 313 nm and it has a high conduction band position because it can only absorb ultraviolet light due to its wide band gap (~ 3.6 eV). However, to grow visible light-active ZnS-based photocatalysts, doping of different elements has been carried out and from the results; it is shown that doping of foreign elements with ZnS successfully enhances the absorbance of ZnS in the visible light region. Yu and his co-workers reported that (Zhang et al. 2011) doped ZnS shows significant enhanced photocatalytic activity under visible light irradiation after the surface moderation of ZnS nanomaterials by CuS.

In the recent work, CuS/ZnS-graphene (CZSG) nanocomposites have been synthesized by a simple green approach until now which is not reported as shown in Table 1. Green nanotechnology (Iravani and Varma 2020; Kanwar et al. 2019) is a term that creates outcomes by following an environmentally friendly path. Several processes have been developed to construct CuS/ZnS-graphene heterojunction such as solvothermal method, sulfuration process, and hydrothermal method (Wang et al. 2016; Shao et al. 2016; Harish et al. 2017) but all of them are chemical ways which have always some drawbacks. So, the green approach (Naghdi et al. 2018; Fahiminia et al. 2019; Nasrollahzadeh and Sajadi 2015, 2016; Nasrollahzadeh et al. 2014, 2015a, b) is the safest path to grow different shaped and dimensioned nanomaterials. It is noticed that the role of graphene in the nanocomposites is to perform as an organic dye-like photosensitizer (Zhang et al. 2012), and upon visible light irradiation, the photo-generated electrons

can move from graphene to the conduction band of ZnS where ZnS is a wide band gap material. In this phenomenon, semiconductors do not participate in the photocatalytic process under visible light irradiation and this type of photocatalytic mechanism is almost distinct from the usual graphene-based semiconductor photocatalysts to date where graphene acts as an electron reservoir to arrest photo-generated electrons from the conduction band of the semiconductor (Ghosh and Sen 2017). Therefore, our research of such a unique photocatalytic reaction mechanism where graphene acts as a photosensitizer (Singh and Khare 2015) as well as with the increase of graphene content shows enhanced photocatalytic response and a decrease of the particle size of the CuS/ZnS NPs grown on the graphene surface.

Materials and methods

Materials

The materials consisted of ultrafine graphite powder (Aldrich), potassium permanganate (Merck), hydrogen peroxide (Merck, 30%), conc. sulfuric acid (Merck, 98% pure), hydrochloric acid (Merck, 30%), zinc sulfate (ZnSO₄, 7H₂O) (Merck), copper sulfate (CuSO₄, 5H₂O) (Merck), green tea leaves, thiourea (SC(NH₂)₂) (Merck), liquor ammonia (NH₃), methylene blue (MB), doubled distilled water, ethanol (Merck), Mueller-Hinton agar (HiMedia), bacterial strains, culture conditions, supplements, and Gram-negative

Table 1 Summary of photocatalytic performance of rGO/graphene-metal sulfide nanocomposites reported in recent papers till date

Sample name	Synthesis route	Amount of catalyst	Concentration of dye	Degradation route	Time (min)	Degradation (%)	Reference (year)
CuS-rGO	Hydrothermal	30 mg	20 mg L ⁻¹ , 50 mL	Visible light	60	99 (H ₂ O ₂ used)	Saranya et al. (2015)
CuS/ZnS-rGO	Hydrothermal via sonochemical	0.1 g	30 mg L ⁻¹ , 100 mL	300W Xe Lamp	50	99 (H ₂ O ₂ used)	Guan et al. (2015)
ZnS-Graphene	Solid-state method	50 mg	10 mg L ⁻¹ , 100 mL	300 W Hg Lamp	80	93 (H ₂ O ₂ not used)	Chen et al. (2015)
ZnS-rGO	Microwave	50 g	1 × 10 ⁻⁴ M	250 W Xe Lamp	180	55 (H ₂ O ₂ not used)	Thangavel et al. (2016)
CuS/ZnS-rGO	Solvothermal with cation exchange resin	0.01 g	50 mg L ⁻¹	300W Xe Lamp	70	99 (H ₂ O ₂ used)	Yang et al. (2017)
CuS-graphene	Microwave	30 mg	5 mg L ⁻¹ , 100 ml	500W Xe Lamp	50	90 (H ₂ O ₂ used)	Zeng et al. (2018)
Cu ₇ S ₄ /ZnS-rGO	Hydrothermal	25 mg	7 mg L ⁻¹ , 100 mL	300 W Xe Lamp	60	99 (H ₂ O ₂ not used)	Li et al. (2019)
CuS-ZnS/rGO	Green Method	10 mg	10 mg L ⁻¹	500 W Xe Lamp	120	91 (H ₂ O ₂ not used)	Present Work

bacteria (*Escherichia coli* BL21 DE3 (*E. coli*), *Aeromonas* sp.) and Gram-positive bacteria (*Bacillus subtilis* (*B. subtilis*), *Staphylococcus aureus* (*S. aureus*), *Cellulosimicrobium* sp.).

Preparation of plant extract

Fresh leaves of green tea were collected from the local market of Burdwan town (W.B) and the resulting mixture was boiled and cooled down at room temperature, followed by severing into small parts of known weight of these plant leaves in 80 mL distilled water. Then, the obtained transparent filtrate was used as a reducing agent after passing through a Whatman 41 filter paper to remove the solid materials.

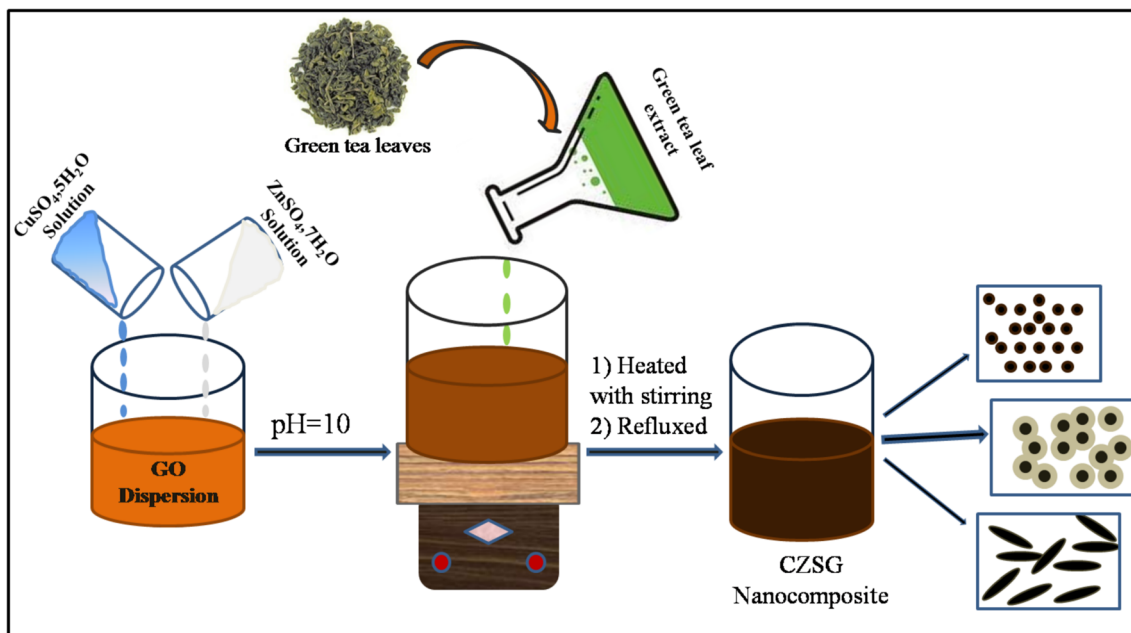
Synthesis of CuS/ZnS-graphene nanocomposite

Here, one of the precursors involved in the reaction is graphene oxide (GO) which was prepared from graphite powder followed by Hummers method (William et al. 1958). In order to develop CZSG nanocomposite, a certain amount of GO was dispersed in 150 mL of water through ultrasonic treatment for 20 min. Then, an aqueous solution of $ZnSO_4 \cdot 7H_2O$ and $CuSO_4 \cdot 5H_2O$ was added at once to the above mentioned solution under stirring condition as shown in Scheme 1. The resulting reaction mixture was stirred vigorously for a few minutes, followed by adjusting the pH of the dispersion to 10 by adding liquor ammonia and then thiourea dropwise. After the addition of green tea extract, the mixture

was agitated by heating at 80 °C for 2 h resulting in deep brown precipitate and transferred to a round bottom flask to get refluxed at 110 °C for 8 h. After completion of the reaction, the black product was collected through centrifugation and was washed using ethanol and doubled distilled water by several times and then dried under vacuum condition at 70 °C temperature. The same procedures were followed to prepare different compositions of the nanocomposites with and without GO and also graphene was prepared using the same protocol without the addition of metal salts. To synthesize different compositions, the weight ratios of the GO, the metal salts, and the sample names are given in Table 2.

Characterization techniques

Powder X-ray diffraction (XRD) measurement was carried out using a powdered sample with X-ray powder diffraction patterns recorded in a Bruker (D8 Advance) diffractometer with Ni-filtered $CuK\alpha$ radiation ($\lambda = 1.5414 \text{ \AA}$). For phase identification, recorded data was compared with standard JCPDS files (Joint Committee of Powder Diffraction System). To study the chemical bonding, Fourier transform infrared (FTIR) study was done by SHIMADZU IR Prestige-21 and the test specimens were prepared by the KBr disk method. The microstructure of the as-synthesized samples was studied by a transmission electron microscope (Model JEOL-1400) and UV-Vis absorption spectra were used to investigate the optical properties of the photocatalysts by recording the data on SHIMADZU UV-1800 spectrophotometer.



Scheme 1 Synthesis diagram of CZSG nanocomposites

Table 2 Weight ratios of ZnSO₄, 7H₂O, CuSO₄, 5H₂O, and GO used for the preparation of CZSG nanocomposites

Sample	Sample name	Amount of ZnSO ₄ , 7H ₂ O (g)	Amount of CuSO ₄ , 5H ₂ O (g)	Amount of GO (g)	Weight ratio (metal salt:GO)
CuS/ZnS-graphene1	CZSG1	1.51	0.7559	0.2036	1:0.09
CuS/ZnS-graphene2	CZSG2	1.51	0.7559	0.4072	1:0.18
CuS/ZnS-graphene4	CZSG4	1.51	0.7559	0.8144	1:0.36
CuS/ZnS	CZS	1.51	0.7559	-	-

Photocatalytic studies

The evaluation of the photocatalytic activity of the as-prepared CZSG nanocomposites was performed at ambient temperature by examining the photo-assisted degradation of MB as the representative dye under visible light illumination. In each photocatalytic experimental procedure, the photocatalyst of a known dosage was added to the fixed amount of dye solution (10 ppm). Then, the mixed dispersion was magnetically stirred in the dark for 30 min before light irradiation at room temperature to ensure the adsorption-desorption equilibrium of MB. Then, visible light source was irradiated to initiate the photocatalytic reaction. The concentration of MB was monitored from time to time using a UV-visible spectrophotometer. The concentration of MB was detected from the decrease in intensity of the absorbance band at around 664 nm by a UV-Vis spectrophotometer. The decomposition efficiency of MB could be determined by the equation:

$$D\% = \frac{(A_0 - A_t)}{A_0} \times 100\% \quad (1)$$

where A_0 refers to the absorption of MB after the adsorption equilibrium is achieved prior to the visible light illumination and A_t is the absorption of MB at time interval t under visible light illumination. Furthermore, photocatalytic kinetics was usually expressed by the following equation:

$$\ln \frac{A_0}{A_t} = kt \quad (2)$$

where k is the apparent pseudo-first-order reaction rate constant and t is the irradiation time.

Recyclability study

To evaluate the photostability of the nanocatalyst, five cycles of dye degradation of MB have been carried out with the most efficient catalyst (CZSG4). After each cycle of photo-degradation test, the MB solution containing used photocatalyst in dispersion state was centrifuged, washed with water, and dried in vacuum, and thus, the used photocatalyst

was separated from the MB solution to be used for the next cycle.

Antibacterial activity

The well diffusion method was used to determine the antibacterial activity of nanocomposites. The bacterial strains (mentioned in the Materials and methods section) were used for this study. Mueller-Hinton agar medium was made by adding 38 g of Mueller-Hinton agar in 1.0 L of Milli-Q water and sterilized by autoclaving for 20 min. One hundred-microliter log phase grown cells from each strain, *E. coli*, *B. subtilis*, *S. aureus*, *Aeromonas* sp., and *Cellulosimicrobium* sp., were spread separately on the solid surface of the plates. The specified volume of sample solutions was placed in the wells and the plates were incubated at 37 °C for 24 h in a bacterial incubator after making the wells of 3 mm in diameter using a sterile cork borer. The zone of inhibition surrounding the wells was noticed by the samples and each zone of inhibition was compared against standard antibiotics of ampicillin (10 µL) and tetracycline (30 µL).

Results and discussion

XRD analysis was applied to determine the crystalline structures of as-prepared CZSG composites. The XRD patterns of well-connected formation of CZSG composites with different GO concentrations are displayed in Fig. 1a. It is obvious that the XRD patterns of CZSG curves exhibit several diffraction peaks at 2θ value at 29.45, 31.79, 32.71, 48.11, 52.51, 58.50, and 59.16 corresponding to (102), (103), (006), (110), (108), (203), and (116) planes of the hexagonal phase of CuS (JCPDS no. 06-0464) (Guan et al. 2015; Shuaia et al. 2018) respectively. Besides, the diffraction peaks at 2θ at 28.53, 47.65, and 56.8 have corresponded to the (111), (220), and (311) planes of the cubic phase of ZnS (JCPDS no. 05-0566) (Abideen and Teng 2018; Huang et al. 2020). There is no peak of graphene oxide (GO) (001) in the composite samples which clearly indicates the successful reduction of GO to graphene.

The existence of different oxygen-containing functional groups on GO and the successful reduction of GO to graphene

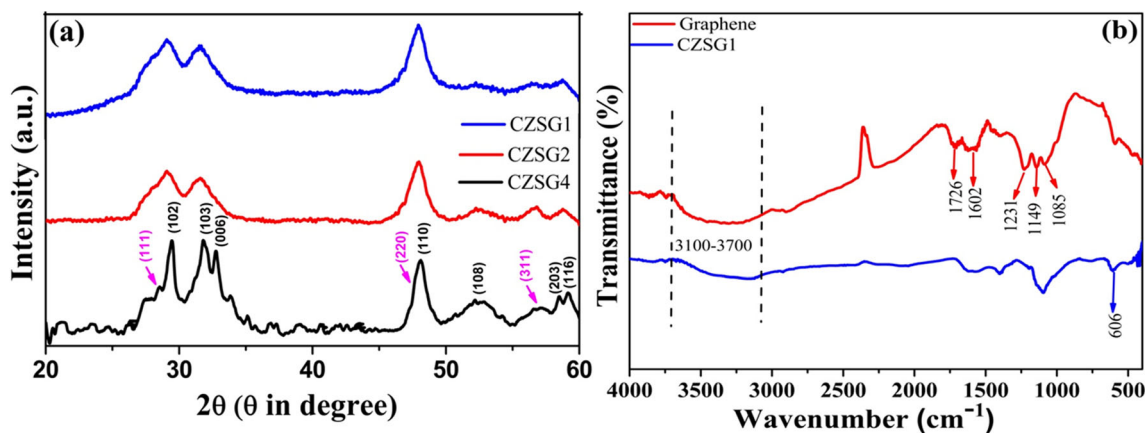


Fig. 1 **a** XRD graphs of CZSG1, CZSG2, and CZSG4 (pink color for ZnS planes and black color for CuS planes and **b** FTIR spectra of graphene and CZSG1

in the CZSG1 nanocomposite was confirmed by FTIR spectroscopy. As shown in Fig. 1b, the FTIR spectrum of GO exhibited several characteristic peaks. The bands at 3450 and 1602 cm^{-1} have belonged to the stretching and bending vibrations of the O–H group (Sennour et al. 2017; Khan et al. 2020). The band at 1726 cm^{-1} is attributed to C=O groups (Abida et al. 2020) and the stretching vibrations at 1231, 1149, and 1085 cm^{-1} are responsible for the C–O bond of epoxy groups (Guan et al. 2014; Liu et al. 2019). The decrease in intensity of these peaks and the appearance of a peak at 606 cm^{-1} (metal-S bond stretching) in the composite material confirm the formation of this nanocomposite (Cao et al. 2019; Dutta et al. 2017).

In Fig. 2a, GO exhibits an π - π^* transition at 230 nm and a hump for n - π^* transition at 305 nm, but after reduction, the π - π^* transition shifts to 270 nm in graphene indicating that some groups are partially removed from the GO surface and the conjugation in the structure is restored (Shams et al. 2019). In CZS sample as shown in Fig. 2b, a hump around 300–380

nm has been found due to CuS/ZnS NPs (Corrado et al. 2010). In the case of CZSG nanocomposite samples, two peaks at around 267–271 nm and 368 nm are responsible due to the π - π^* transition in graphene and the formation of CZS NPs on the graphene surface (Devi et al. 2015; Reddy et al. 2014).

The optical band gap study has been investigated to ensure the band gap values in the nanocomposites. The band gap values for the nanocomposites have been explored from the optical absorption phenomenon which obeys Tauc’s formula (Zanatta 2019; Morales et al. 2019). The value of the band gap can be calculated using the fundamental absorption which corresponds to the electron jump from the valance band to the conduction band. The absorption coefficient (α) and the incident photon energy ($h\nu$) are connected with the Tauc’s formula given by the equation:

$$(\alpha h\nu)^n = K(h\nu - E_g) \tag{3}$$

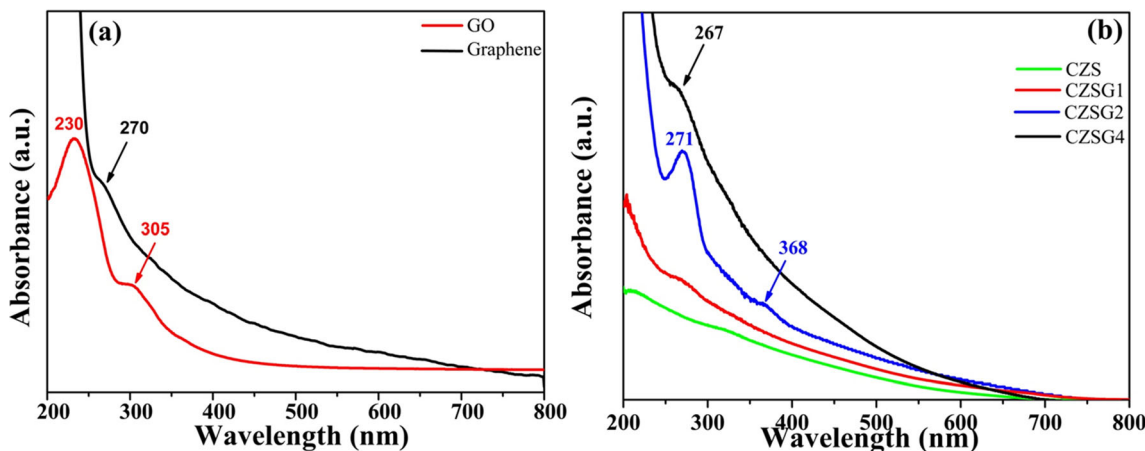


Fig. 2 UV-Vis spectra of **a** GO and graphene **b** CZSG nanocomposites

where $h\nu$ is the photon energy, α is the absorption coefficient, K is a constant, E_g is the band gap energy, and the value of n is 2 for direct allowed transitions while it is $\frac{1}{2}$ for the indirect allowed transition. The variation of $(\alpha h\nu)^2$ vs. $h\nu$ for the samples reveals that the exploration of the linear portion to the $h\nu$ axis gives the energy gap of the direct band gap (Abdel-Kader and Mohamed 2020). From Fig. 3, it is shown that the values of the direct band gap for the CZS, CZSG1, CZSG2, and CZSG4 are 3.04, 2.93, 2.90, and 2.87 eV, respectively, which clearly indicate a band gap narrowing of the CZS sample after the coupling with graphene in CZSG nanocomposites. According to a literature study (Wang et al. 2015a, b; Lonkar et al. 2018), this result can be ascribed due to the hybridization of carbon materials in which doping of graphene into the CZS nanoparticles originates mid-gap energy levels resulting in a decrease in band gap energy.

With the increase of graphene content in the CZSG nanocomposites, the particle size decreases as shown in Fig. 4. The approximate sizes of the samples CZSG1, CZSG2, and CZSG4 are 175–215 nm, 125, and 9 nm respectively. With the increase of the graphene content in the nanocomposite samples, the NP size grown on the graphene surface follows the order CZSG1 > CZSG2 > CZSG4. This is because of the

fact that there are many negative groups on GO which act as good nucleation sites for the NP growth (Stanek et al. 2016; Paranthaman et al. 2019). So, with the increase of the GO content, nucleation sites increase, and the probability of agglomeration decreases, as a result, the size of the NPs decreases (Khan et al. 2015; Estelléa et al. 2018).

Photocatalytic study

It was believed that the photocatalytic activity of a photocatalyst is enhanced depending on the (i) separation efficiency of the photo-excited electron-hole pairs and the (ii) amount of the reactive oxygen species (ROS) (Riente and Noël 2019). Under visible light irradiation, ZnS cannot respond due to a large band gap value (Wang et al. 2015a, b) but CuS is active in this condition (Adhikari et al. 2017). Therefore, a heterojunction is formed between ZnS and CuS to transfer the photo-generated electrons from CB of CuS to CB of ZnS leaving the holes in the VB of CuS (Shao et al. 2016) and the resulting suppression of recombination of electron-hole pairs occurs and thus the photocatalytic activity is increased (path (I)) as shown in Scheme 2. In Fig. 5a, the bare CZS sample shows the photocatalytic activity 63.66%

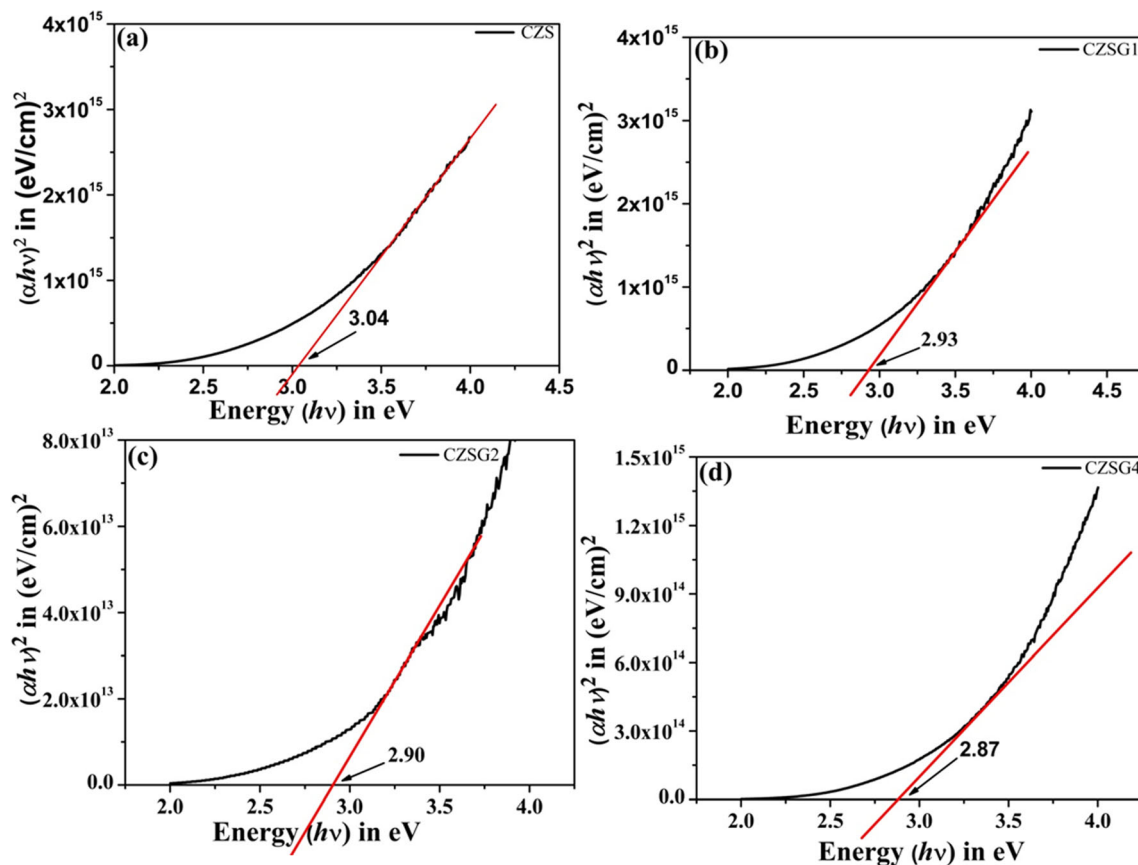


Fig. 3 UV-Vis absorption data fitted by Tauc's formula for direct band gap of **a** CZS, **b** CZSG1, **c** CZSG2, and **d** CZSG4 nanocomposites

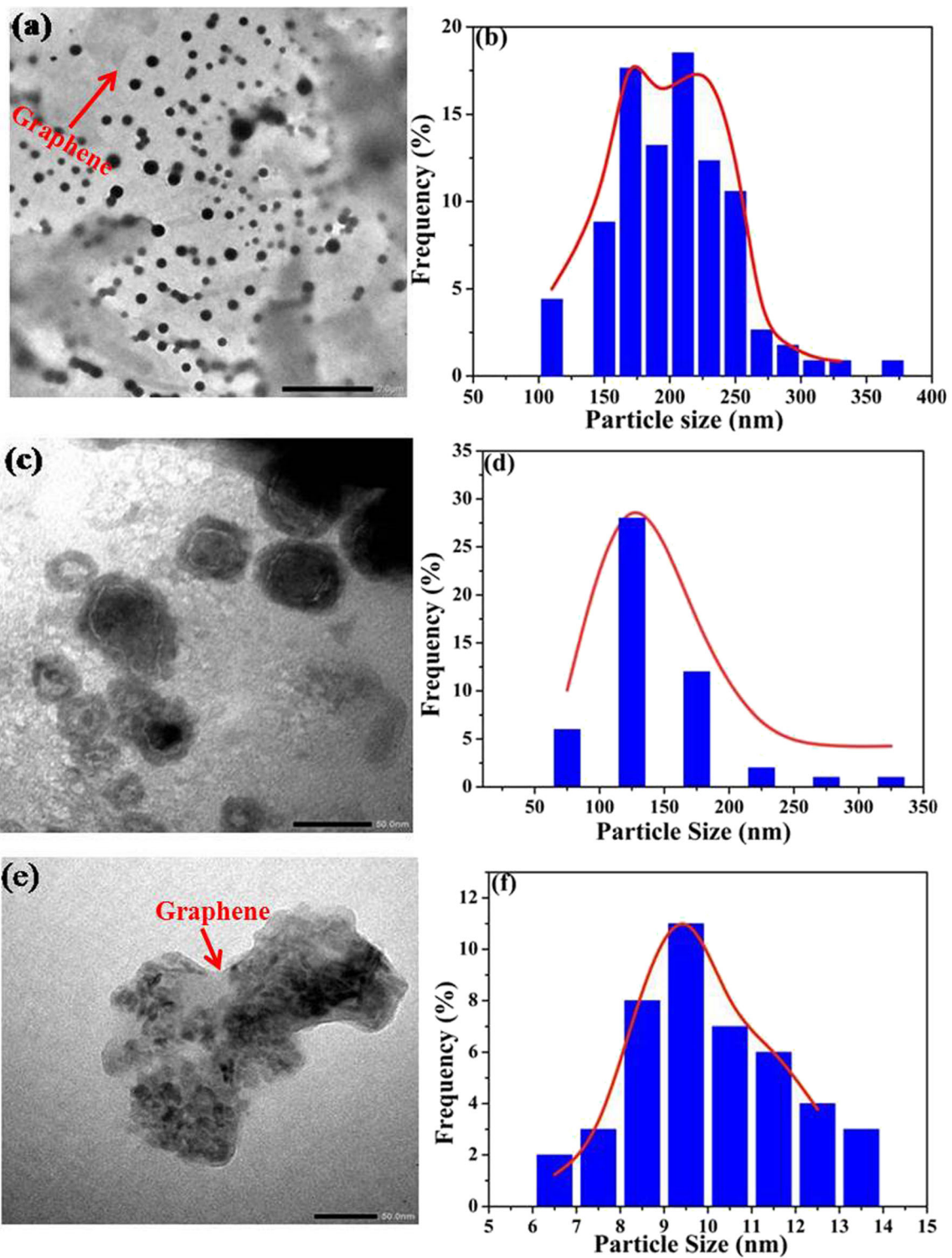
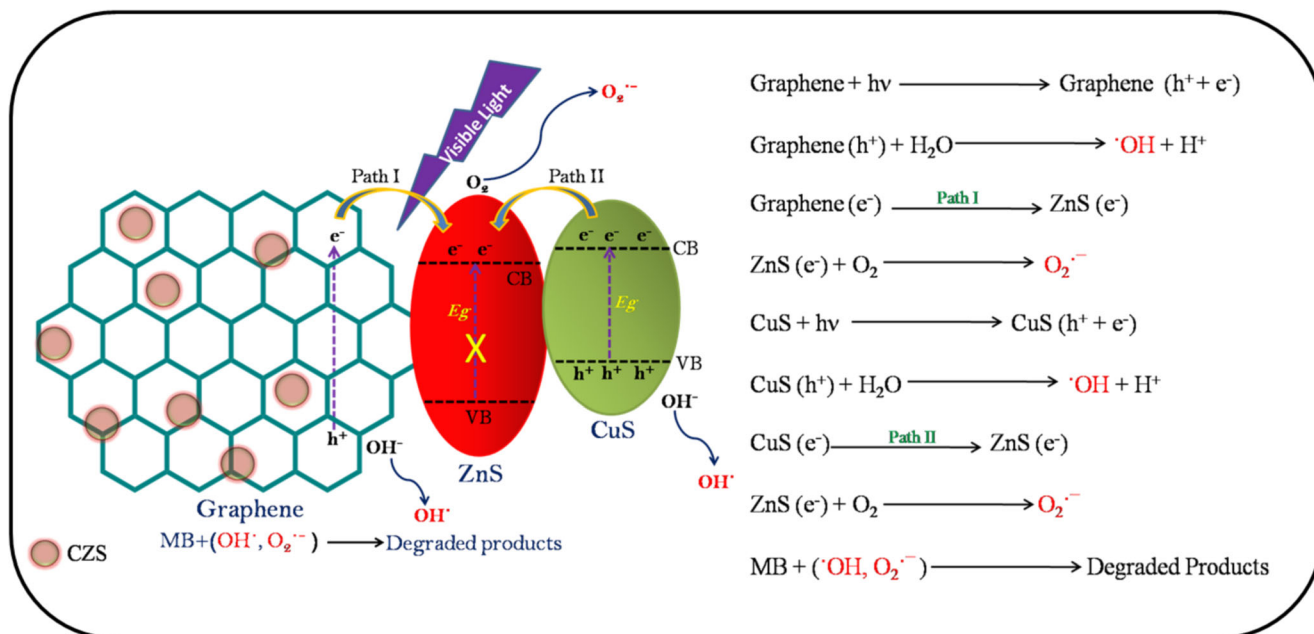


Fig. 4 TEM images of **a** CZSG1, **c** CZSG2, and **e** CZSG4 nanocomposites and **b**, **d**, and **f** are size distribution graphs of CZSG1, CZSG2, and CZSG4 nanocomposites



Scheme 2 a, b Pictorial and schematic representation of photocatalytic mechanism respectively

within 100 min, but after the incorporation of graphene with the binary CZS nanocomposite, the enhanced photocatalytic activities become 79.71%, 87.48%, and 90.21% in the case of nanocomposite samples CZSG1, CZSG2, and CZSG4 respectively (Fig. 5b–d). The bare CZS exhibited less photocatalytic activity than the CZSG nanocomposites due to the aggregation of CZS NPs which results in larger sized NPs. Actually, graphene acts as an organic dye-like macromolecular ‘photosensitizer’ (Feng et al. 2014; Gálvez et al. 2019), where under visible light irradiation, the electrons on the highest occupied molecular orbital (HOMO) of graphene were at first excited to the lowest unoccupied molecular orbital (LUMO) of graphene and then the photo-excited electrons in graphene move to the CB of ZnS, resulting in the separation of electron-hole pairs. Thus, in CB of ZnS, the number of photo-excited electrons has been increased after the addition of graphene in CZSG nanocomposite (path (II)). For this reason, with the increase of graphene content, the photocatalytic activity gradually increases in the graphene-based nanocomposite samples than that of bare CZS nanocatalyst. The rate constants of the MB degradation for the samples are given in Table 3.

Recyclability tests

Since CZSG4 nanocomposite shows excellent photodegradation efficiency, the photocatalytic stability was investigated using this composite by recycling tests (Rajendran et al. 2016). The results of the recyclability test are shown in Fig. 6a, which shows a slight decrease in its catalytic performance after each cycle. This photocatalyst exhibits excellent

photostability even after five cycles which further confirms the excellent stability of the nanocomposite under visible light irradiation.

Antibacterial activity

In the present study, the antibacterial activity of the synthesized samples was tested by a well diffusion method using bacterial strain *E. coli* BL21 DE3 Gram-negative, *S. aureus* Gram-positive and *B. subtilis* Gram-positive, *Aeromonas* sp. Gram-negative, and *Cellulosimicrobium* sp. Gram-positive. The CZS (P), CZSG1 (Q), CZSG2 (R), and CZSG 4 (S) were promising in exhibiting their ability to destroy *B. subtilis*, a Gram-positive bacterium. The zone of inhibition was measured for P, Q, R, and S at 50 mg mL⁻¹ concentration, shown in Table 5. The antimicrobial activities of P, Q, R, and S were compared against two standard antibiotics (Fig. 7 and Table 4)

Table 3 Comparison of the degradation efficiency, the rate constant, and relative correlation coefficient of different as-prepared nanocomposite samples

Sample	% of Degradation	Rate constant (min ⁻¹)	R ² value
CZS	63.66%	0.010122	0.7932
CZSG1	79.71%	0.01595	0.9800
CZSG2	87.48%	0.02078	0.9624
CZSG4	90.21%	0.02323	0.9827

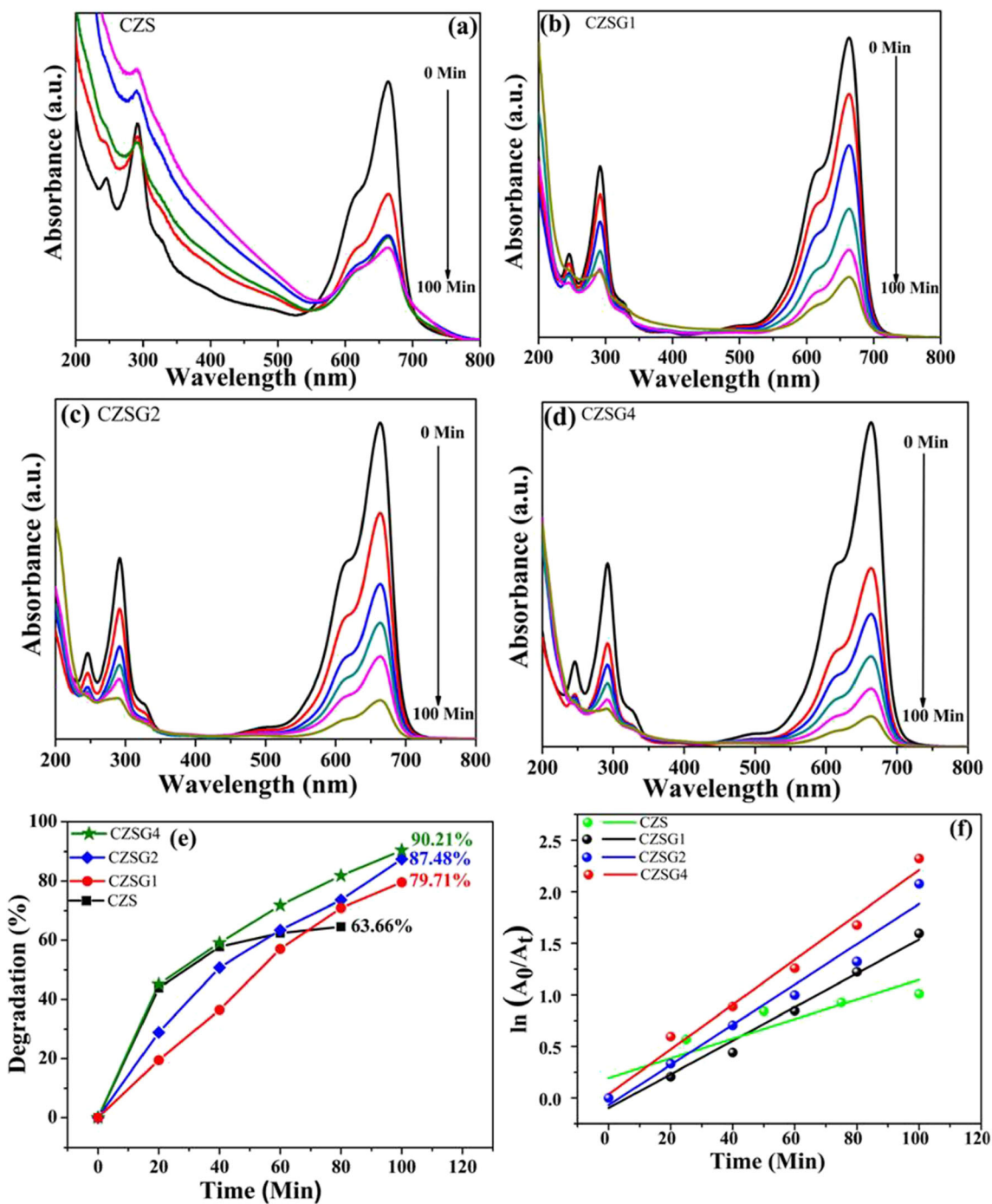


Fig. 5 Absorption spectra of MB solution in the presence of **a** CZS, **b** CZSG1, **c** CZSG2 and **d** CZSG4 respectively under visible light irradiation. **e, f** Photocatalytic degradation of MB and rate kinetics in the presence of different CZSG photocatalysts under visible light irradiation

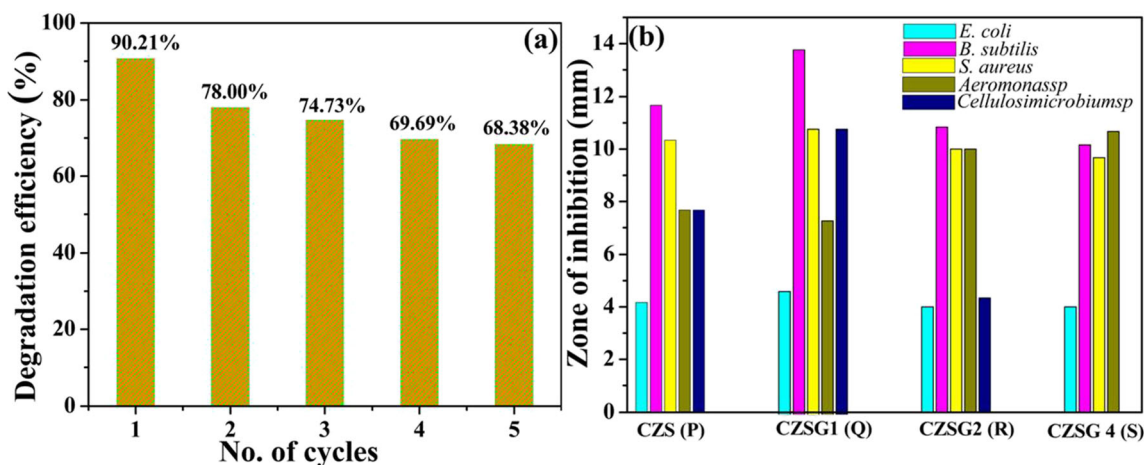


Fig. 6 a Recyclability tests of CZSG4 nanocatalyst for degradation of MB dye. b Bar diagram showing zone of inhibition (in mm) introduced by CZS (P), CZSG1 (Q), CZSG2 (R), and CZSG4 (S) against various microorganisms

ampicillin and tetracycline. As shown in Fig. 6b, it was clear from the study that P, Q, R, and S nanoparticles have good antimicrobial activities on bacterial strains (Table 5).

± Standard deviation

Conclusions

In summary, CuS/ZnS-graphene nanocomposites with different graphene content have been fabricated via a simple greener approach and different characterization techniques

Table 5 Antibacterial activities of P, Q, R, and S NPs

Serial no.	Bacterial strain	Concentration (mg mL ⁻¹)	Volume (μL)	Zone of inhibition (mm in diameter)
1(P)	<i>E. coli</i>	50	30	4.17 ± 0.29
	<i>B. subtilis</i>	50	30	11.67 ± 0.58
	<i>S. aureus</i>	50	30	10.34 ± 0.58
	<i>Aeromonas sp.</i>	50	30	7.67 ± 0.58
	<i>Cellulosimicrobium sp.</i>	50	30	7.67 ± 0.58
2(Q)	<i>E. coli</i>	50	30	4.67 ± 0.58
	<i>B. subtilis</i>	50	30	13.84 ± 0.29
	<i>S. aureus</i>	50	30	10.84 ± 0.29
	<i>Aeromonas sp.</i>	50	30	7.34 ± 0.58
	<i>Cellulosimicrobium sp.</i>	50	30	10.84 ± 0.29
3(R)	<i>E. coli</i>	50	30	4 ± 0
	<i>B. subtilis</i>	50	30	10.84 ± 0.29
	<i>S. aureus</i>	50	30	10 ± 0
	<i>Aeromonas sp.</i>	50	30	10 ± 0
	<i>Cellulosimicrobium sp.</i>	50	30	4.34 ± 0.58
4(S)	<i>E. coli</i>	50	30	4 ± 0
	<i>B. subtilis</i>	50	30	10.16 ± 0.29
	<i>S. aureus</i>	50	30	9.67 ± 0.58
	<i>Aeromonas sp.</i>	50	30	10.67 ± 0.58
	<i>Cellulosimicrobium sp.</i>	50	30	-

Table 4 Antibacterial activity of standard antibiotics against bacterial strains

Bacterial strain	Concentration of antibiotics (mg mL ⁻¹)	Zone of inhibition for antibiotics (mm in diameter)	
		Ampicillin	Tetracycline
<i>E. coli</i>	10	23.67 ± 0.58	25.84 ± 0.29
<i>B. subtilis</i>	10	23.34 ± 0.58	24.84 ± 0.29
<i>S. aureus</i>	10	29.67 ± 0.58	24.67 ± 0.58
<i>Aeromonas</i> sp.	10	-	28 ± 0
<i>Cellulosimicrobium</i> sp.	10	26.34 ± 0.58	28.34 ± 0.58

confirm the synthesis of these nanocomposites. Microscopic study reveals that with the increase of the amount of graphene in the nanocomposites, the particle size of the CZS nanoparticles decreases due to a decrease in aggregation in high surface area graphene sheet and band gap energy also diminishes. The CZSG nanocomposites can act as visible light photocatalysts towards organic dye degradation. It has been exemplified that the

visible light-driven nanocomposites/photocatalysts show remarkably efficient dye degradation capability due to the role of graphene as a photosensitizer. Due to having promising effects in various strains of microorganisms, the nanocomposites can act as potential antibacterial agents. These findings could assist to fabricate new graphene-based photocatalysts with better photocatalytic performance and stability in visible light irradiation.

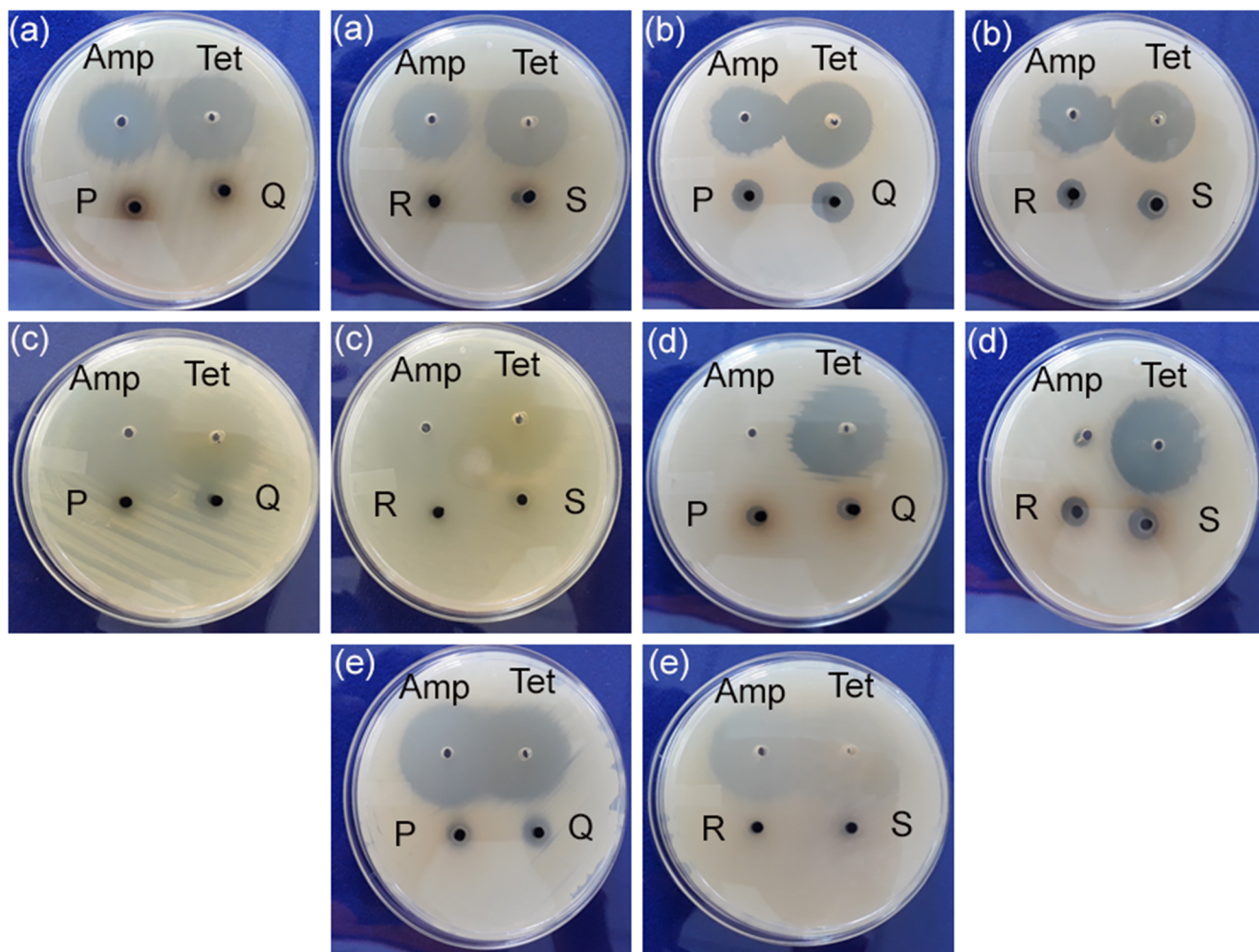


Fig. 7 Antibacterial activity of CZS, CZSG1, CZSG2, and CZSG4 (P, Q, R, and S in the picture respectively) nanocomposites against **a** *E.coli*, **b** *B. subtilis*, **c** *S. aureus*, **d** *Aeromonas* sp., and **e** *Cellulosimicrobium* sp. respectively

Acknowledgments We acknowledge the University Science Instrumentation Center (USIC) for TEM facility.

Author contribution Piu Das: Writing (original draft), writing (review and editing), conceptualization, methodology, and investigation. Kartik Tantubay: Validation, conceptualization, data curation, visualization, and funding acquisition. Raktim Ghosh: Methodology and validation. Somasri Dam: Formal analysis and funding acquisition. Moni Baskey Sen: Supervision, writing, and conceptualization.

Funding P.D acknowledges Bagati Shib Chandra Banerjee Girls' High School, Hooghly, and K.T acknowledges Swami Vivekananda Merit Cum Means Scholarship (Non-NET Junior Research Fellowship), Higher Education Department, Govt. of West Bengal for financial support for giving permission to continue her research work. R.G. and S. D. are thankful to DAE-BRNS project (37 (1)/20/15/2014-BRNS/808) for financial support.

Data availability The data that support the findings of this study are available from authors.

Declarations

Ethics approval and consent to participate All procedures performed in studies involving human participants were in accordance with the ethical standards of the institutional and/or national research committee and with the 1964 Helsinki declaration and its later amendments or comparable ethical standards. All participants voluntarily agreed to participate in this research study.

Consent for publication All participants voluntarily agreed to publish their research work in Springer journal.

Competing interests The authors declare no competing interests.

References

- Abdel-Kader MH, Mohamed MB (2020) Exploring the direct effect of intermediate band semiconductor materials on the structural, thermal and optical properties of PMMA nanocomposite. *Appl Phys A Mater Sci Process* 126:1–11
- Abida K, Chudasama B, Ali A (2020) Development and functionalization of magnetic nanoparticles as stable and reusable catalysts for triacetin synthesis. *New J Chem* 44:9365–9376
- Abideen ZU, Teng F (2018) Enhanced photochemical activity and stability of ZnS by a simple alkaline treatment approach. *Cryst Eng Comm* 20:7866–7879
- Adhikari S, Sarkar D, Madras G (2017) Hierarchical design of CuS architectures for visible light photocatalysis of 4-Chlorophenol. *ACS Omega* 2:4009–4021
- Akbari A, Sabouri Z, Hosseini HA, Hashemzadeh A, Khatami M, Darroudi M (2020) Effect of nickel oxide nanoparticles as a photocatalyst in dyes degradation and evaluation of effective parameters in their removal from aqueous environments. *Inorg Chem Commun* 115:107867–107877
- Cao F, Wu L, Zhang X, Li S, Wang C, Zhen W, Jiang X (2019) Dynamic surface properties of PEG-coated CuS nanoparticles alter their interaction with cells as revealed by surface-enhanced infrared spectroscopy. *Nanoscale Adv* 1:4268–4276
- Chen F, Cao Y, Jia D, Liu A (2015) Solid-state synthesis of ZnS/graphene nanocomposites with enhanced photocatalytic activity. *Dyes Pigments* 120:8–14
- Corrado C, Hawker M, Livingston G, Medling S, Bridges F, Zhang JZ (2010) Enhanced Cu emission in ZnS: Cu, Cl/ZnS core-shell nanocrystals. *Nanoscale* 2:1213–1221
- Das P, Ghosh S, Ghosh R, Dam S, Sen MB (2018) Madhuca longifolia plant mediated green synthesis of cupric oxide nanoparticles: a promising environmentally sustainable material for waste water treatment and efficient antibacterial agent. *J Photochem Photobiol B Biol* 189:66–73
- Devi MM, Sahu SR, Mukherjee P, Sen P, Biswas K (2015) Graphene: a self-reducing template for synthesis of graphene-nanoparticles hybrids. *RSC Adv* 5:62284–62289
- Dutta S, Chatterjee S, Mukherjee I, Saha RN, Singh BP (2017) Fabrication of ZnS hollow spheres and RGO-ZnS nanocomposite using cysteamine as novel sulfur source: photocatalytic performance on industrial dyes and effluent. *Ind Eng Chem Res* 56(16):4768–4778
- Estelléa P, Cabaleiro D, Żyłał G, Lugob L, Murshed SMS (2018) Current trends in surface tension and wetting behavior of nanofluids. *Renew Sust Energ Rev* 94:931–944
- Fahiminia M, Shamabadi NS, Nasrollahzadeh M, Sajadi SM (2019) Phytosynthesis of Cu/rGO using Euphorbia cheiradenia Boiss extract and study of its ability in the reduction of organic dyes and 4-nitrophenol in aqueous medium. *IET Nanobiotechnology* 13:202–213
- Feng Y, Feng N, Wei Y, Zhang G (2014) An in situ gelatin-assisted hydrothermal synthesis of ZnO-reduced graphene oxide composites with enhanced photocatalytic performance under ultraviolet and visible light. *RSC Adv* 4:7933–7943
- Feng C, Meng X, Song X, Feng X, Zhao Y, Liu G (2016) Controllable synthesis of hierarchical CuS/ZnS hetero-nanowires as high performance visible-light photocatalysts. *RSC Adv* 6:110266–110273
- Fujishima A, Honda K (1972) Electrochemical photolysis of water at a semiconductor electrode. *Nature* 238:37–38
- Gálvez HEG, Alvarado-Beltrán CG, Almaral-Sánchez JL, Hurtado-Maciasb A, Fontecha AMG, Luqued PA, Castro-Beltrán (2019) A graphene role in improved solar photocatalytic performance of TiO₂-RGO nanocomposite. *Chem Phys* 521:35–43
- Ghosh S, Sen MB (2017) Enhanced sunlight photocatalytic activity of silver nanoparticles decorated on reduced graphene oxide sheet. *Korean J Chem Eng* 34:2079–2085
- Guan LZ, Wan YJ, Gong LX, Yan D, Tang LC, Wu LB, Jiang JX, La GQ (2014) Toward effective and tunable interphases in graphene oxide/epoxy composites by grafting different chain lengths of polyetheramine onto graphene oxide. *J Mater Chem A* 2:15058–15069
- Guan XH, Yang L, Guan X, Wang GS (2015) Synthesis of a flower-like CuS/ZnS nanocomposite decorated on reduced graphene oxide and its photocatalytic performance. *RSC Adv* 5:36185–36191
- Harish S, Archana J, Navaneethan M, Ponnusamy S, Singh A, Gupta V, Aswal DK, Ikeda H, Hayakawa Y (2017) Synergetic effect of CuS@ZnS nanostructures on photocatalytic degradation of organic pollutant under visible light irradiation. *RSC Adv* 7:34366–34375
- Huang HB, Fang ZB, Yu K, Lü J, Cao R (2020) Visible-light-driven photocatalytic H₂ evolution over CdZnS nanocrystal solid solutions: interplay of twin structures, sulfur vacancies and sacrificial agents. *J Mater Chem A* 8:3882–3891
- Iravani S, Varma RS (2020) Greener synthesis of lignin nanoparticles and their applications. *Green Chem* 22:612–636
- Kanwar R, Rathee J, Salunke DB, Mehta SK (2019) Green nanotechnology-driven drug delivery assemblies. *ACS Omega* 4: 8804–8815
- Khan M, Tahir MN, Adil SF, Khan HU, Siddiqui MRH, Al-warthan AA, Tremel W (2015) Graphene based metal and metal oxide nanocomposites: synthesis, properties and their applications. *J Mater Chem A* 3:18753–18808
- Khan I, Khan AA, Khan I, Usman M, Sadiq M, Ali F, Saeed K (2020) Investigation of photocatalytic potential enhancement of silica

- monolith decorated tin oxide nanoparticles through experimental and theoretical studies. *New J Chem* 44:13330–13343
- Li X, Cao J, Yang L, Wei M, Liu X, Liu Q, Hong Y, Zhou Y, Yang J (2019) One-pot synthesis of ZnS nanowires/Cu₇S₄ nanoparticles reduce graphene oxide nanocomposites for supercapacitor and photocatalytic applications. *Dalton Trans* 48:2442–2454
- Liang C, Niu CG, Wen XJ, Yang SF, Shen MC, Zeng GM (2017) Effective removal of colourless pollutants and organic dyes by Ag@AgCl nanoparticles modified CaSn(OH)₆ composite under visible light irradiation. *New J Chem* 41:5334–5346
- Liu H, Hu X, Guo H, Zhao J, Li F, Zhu D, Liu S (2019) One-step reducing and dispersing graphene oxide via hydroxypropyl hydrazine and its applications in Cu²⁺ removal. *Phys Chem Chem Phys* 21:10947–10954
- Lonkar SP, Pillai VV, Alhassan SM (2018) Facile and scalable production of heterostructured ZnS-ZnO/graphene nano-photocatalysts for environmental remediation. *Sci Rep* 8:13401–13414
- Ma D, Shi JW, Zou Y, Fan Z, Ji X, Niu C (2017) Highly efficient photocatalyst based on a CdS quantum dots/ZnO nanosheets 0D/2D heterojunction for hydrogen evolution from water splitting. *ACS Appl Mater Interfaces* 9(30):25377–25386
- Morales AE, Ruiz-Lopez II, Ruiz-Peralta M-dL, Tepech-Carrillo L, Sanchez-Cantu M, Moreno-Orea JE (2019) Automated method for the determination of the band gap energy of pure and mixed powder samples using diffuse reflectance spectroscopy. *Heliyon* 5:1–19
- Mosleh S, Dashtian K, Ghaedi M, Amir MA (2019) Bi₂WO₆/Ag₂S/ZnS Z-scheme heterojunction photocatalyst with enhanced visible-light photoactivity towards the degradation of multiple dye pollutants. *RSC Adv* 9:30100–30111
- Naghdi S, Sajjadi M, Nasrollahzadeh M, Rhee KY, Sajadi SM, Jaleh B (2018) *Cuscuta reflexa* leaf extract mediated green synthesis of the Cu nanoparticles on graphene oxide/manganese dioxide nanocomposite and its catalytic activity toward reduction of nitroarenes and organic dyes. *J Taiwan Inst Chem Eng* 86:158–173
- Nasrollahzadeh M, Sajadi SM (2015) Preparation of Au nanoparticles by *Anthemis xylopoda* flowers aqueous extract and their application for alkyne/aldehyde/amine A³-type coupling reactions. *RSC Adv* 5:46240–46246
- Nasrollahzadeh M, Sajadi SM (2016) Preparation of Pd/Fe₃O₄ nanoparticles by use of *Euphorbia stracheyi* Boiss root extract: a magnetically recoverable catalyst for one-pot reductive amination of aldehydes at room temperature. *J Colloid Interface Sci* 464:147–152
- Nasrollahzadeh M, Sajadi SM, Rostami-Vartooni A, Khalaj M (2014) Journey on greener pathways: use of *Euphorbia condylocarpa* M. bieb as reductant and stabilizer for green synthesis of Au/Pd bimetallic nanoparticles as reusable catalysts in the Suzuki and Heck coupling reactions in water. *RSC Adv* 4:43477–43484
- Nasrollahzadeh M, Sajadi SM, Maham M (2015a) *Tamarix gallica* leaf extract mediated novel route for green synthesis of CuO nanoparticles and their application for N-arylation of nitrogen-containing heterocycles under ligand-free conditions. *RSC Adv* 5:40628–40635
- Nasrollahzadeh M, Sajadi SM, Rostami-Vartooni A (2015b) Green synthesis of CuO nanoparticles by aqueous extract of *Anthemis nobilis* flowers and their catalytic activity for the A³ coupling reaction. *J Colloid Interface Sci* 459:183–188
- Nasrollahzadeh M, Jaleh B, Baran T, Varma RS (2020) Efficient degradation of environmental contaminants using Pd-RGO nanocomposite as a retrievable catalyst. *Clean Techn Environ Policy* 22:325–335
- Paranthaman T, Dey MD, Das SK (2019) Biofabrication of supported metal nanoparticles: exploring the bioinspiration strategy to mitigate the environmental challenges. *Green Chem* 21:5469–5500
- Prabhu YT, Rao VN, Shankar MV, Sreedhar B, Pal U (2019) The facile hydrothermal synthesis of CuO@ZnO heterojunction nanostructures for enhanced photocatalytic hydrogen evolution. *New J Chem* 6794–6805
- Rajendran S, Khan MM, Gracia F, Qin J, Gupta VK, Arumainathan S (2016) Ce³⁺-ion-induced visible-light photocatalytic degradation and electrochemical activity of ZnO/CeO₂ nanocomposite. *Sci Rep* 6:1–11
- Reddy DA, Ma R, Choi MY, Kima TK (2014) Reduced graphene oxide wrapped ZnS–Ag₂S ternary composites synthesized via hydrothermal method: applications in photocatalyst degradation of organic pollutants. *Appl Surf Sci* 324:1–18
- Riente P, Noël T (2019) Application of metal oxide semiconductors in light-driven organic transformations. *Catal Sci Technol* 9:5186–5232
- Saranya M, Ramachandran R, Kollu P, Jeong SK, Grace AN (2015) A template-free facile approach for the synthesis of CuS-rGO nanocomposites towards enhanced photocatalytic reduction of organic contaminants and textile effluents. *RSC Adv* 5:15831–15840
- Sennour R, Shiao TC, Arus VA, Tahir MN, Bouazizi N, Roy R, Azzouz A (2017) Cu⁰-Loaded organo-montmorillonite with improved affinity towards hydrogen: an insight into matrix–metal and non-contact hydrogen–metal interactions. *Phys Chem Chem Phys* 19:29333–29343
- Shams M, Guiney LM, Huang L, Ramesh M, Yang X, Hersam MC, Chowdhury I (2019) Influence of functional groups on the degradation of graphene oxide nanomaterials. *Environ Sci Nano* 6:2203–2214
- Shao YB, Wang LH, Huang JH (2016) ZnS/CuS nanotubes for visible light-driven photocatalytic hydrogen generation. *RSC Adv* 6:84493–84499
- Shuaia X, Shenb W, Lia X, Houa Z, Kea S, Shia G, Xua C, Fan D (2018) Cation exchange synthesis of CuS nanotubes composed of nanoparticles as low-cost counter electrodes for dye-sensitized solar cells. *Mater Sci Eng B* 227:74–79
- Singh S, Khare N (2015) Reduced graphene oxide coupled CdS/CoFe₂O₄ ternary nanohybrid with enhanced photocatalytic activity and stability: A potential role of reduced graphene oxide as a visible light responsive photosensitizer. *RSC Adv* 5:96562–96572
- Stanek KS, Kisielewska A, Ginter J, Baluszynska K, Pivonski I (2016) Elucidation of the function of oxygen moieties on graphene oxide and reduced graphene oxide in the nucleation and growth of silver nanoparticles. *RSC Adv* 6:60056–60067
- Tang Y, Liu X, Ma C, Zhou M, Huo P, Yu L, Pan J, Shia W, Yan Y (2015) Enhanced photocatalytic degradation of tetracycline antibiotics by reduced graphene oxide–CdS/ZnS heterostructure photocatalysts. *New J Chem* 39:5150–5160
- Tantubay K, Das P, Sen MB (2020) Ternary reduced graphene oxide–CuO/ZnO nanocomposite as a recyclable catalyst with enhanced reducing capability. *J Environ Chem Eng* 8:103818–103824
- Thangavel S, Krishnamoorthy K, Kimb SJ, Venugopal G (2016) Designing ZnS decorated reduced graphene-oxide nanohybrid via microwave route and their application in photocatalysis. *J Alloys Compd* 683:456–462
- Wang G, Huang B, Li Z, Lou Z, Wang Z, Dai Y, Whangbo MH (2015a) Synthesis and characterization of ZnS with controlled amount of S vacancies for photocatalytic H₂ production under visible light. *Sci Rep* 5(8544):1–7
- Wang F, Zheng M, Zhu C, Zhang B, Ma WCL, Shen W (2015b) Visible light photocatalytic H₂ production activity of wide band gap ZnS nanoparticles based on the photosensitization of graphene. *Nanotechnol* 26:345402–345410
- Wang L, Chen H, Xiao L, Huang J (2016) CuS/ZnS hexagonal plates with enhanced hydrogen evolution activity under visible light irradiation. *Powder Technol* 288:103–108
- Wang Z, Huang J, Mao J, Guo Q, Chen Z, Lai Y (2020) Metal-organic frameworks and their derivatives with graphene composites: Preparation and applications in electrocatalysis and photocatalysis: a review. *J Mater Chem A* 8:2934–2961

- William S, Hummers J, Offeman RE (1958) Preparation of graphitic oxide. *J Am Chem Soc* 80:1339
- Yang L, Guan X, Wang GS, Guan XH, Jia B (2017) Synthesis of ZnS/CuS nanospheres loaded on reduced graphene oxide as high-performance photocatalysts under simulated sunlight irradiation. *New J Chem* 41:5732–5744
- Yek SM, Azarifar D, Nasrollahzadeh M, Bagherzadeh M, Shokouhimehr M (2020) Heterogenized Cu(II) complex of 5-aminotetrazole immobilized on graphene oxide nanosheets as an efficient catalyst for treating environmental contaminants. *Sep Purif Technol* 247:116952–116962
- Zanatta AR (2019) Revisiting the optical bandgap of semiconductors and the proposal of a unified methodology to its determination. *Sci Rep* 9(11225):1–12
- Zeng B, Liu W, Zeng W, Jin C (2018) Graphene decorated with hierarchical CuS nanoplates: enhanced photocatalytic performance. *Nano Brief Rep Rev* 13:1850029–1850035
- Zhang J, Yu JG, Zhang YM, Li Q, Gong JR (2011) Visible light photocatalytic H₂-production activity of CuS/ZnS porous nanosheets based on photoinduced interfacial charge transfer. *Nano Lett* 11:4774–4779
- Zhang Y, Zhang N, Tang ZR, Xu YJ (2012) Graphene transforms wide band gap ZnS to a visible light photocatalyst. The new role of graphene as a macromolecular photosensitizer. *ACS Nano* 6(11):9777–9789

Publisher's note Springer Nature remains neutral with regard to jurisdictional claims in published maps and institutional affiliations.